SCIENCE CHINA
Information Sciences

• RESEARCH PAPER •

December 2023, Vol. 66 222201:1–222201:15
https://doi.org/10.1007/s11432-022-3767-2

Identification of Hammerstein-Wiener model with discontinuous input nonlinearity

A. BROURI[1], F. Z. EL MANSOURI[1*], F. Z. CHAOUI[2], C. ABDELAALI[1] & F. GIRI[3]

[1]*ENSAM, Moulay Ismail University, Meknes* 50000*, Morocco;*
[2]*ENSAM, University Mohammed V, Rabat* 10000*, Morocco;*
[3]*Normandie Universite, Caen* 14118*, France*

Received 5 November 2022/Revised 21 January 2023/Accepted 7 March 2023/Published online 23 November 2023

Abstract This paper deals with the identification of Hammerstein-Wiener models with an irregular function in the input block. These models comprise a set of linear segments. The linear time invariant (LTI) block may be parametric or nonparametric. The nonlinearity of the output can be any continuous function of arbitrary shape; it is not necessarily assumed to be invertible. Subsequently, sine inputs will be used to identify the system parameters. First, the output nonlinearity is determined by filtering the system output and varying the phase of a given reference sine signal; second, the parameters of the linear block can be determined for any frequency; and finally, the input nonlinearity can be obtained by changing the offset and amplitude of the input sine signal.

Keywords nonlinear systems, nonlinear systems identification, Hammerstein-Wiener models, discontinuous nonlinearities, hard nonlinearities

Citation Brouri A, El Mansouri F Z, Chaoui F Z, et al. Identification of Hammerstein-Wiener model with discontinuous input nonlinearity. Sci China Inf Sci, 2023, 66(12): 222201, https://doi.org/10.1007/s11432-022-3767-2

1 Introduction

The identification problem of block-oriented nonlinear systems has recently garnered considerable research interest [1–4]. The identification of the system is a crucial step in control and stabilization [5]. Moreover, the identification of block-oriented systems often deals with smooth nonlinearity or considers nonlinearity described by a set of known basis functions [6, 7]. It must be noted that several open problems continue to persist in the identification of block-oriented nonlinear systems, especially when a hard (discontinuous) nonlinearity is employed [8, 9]. Various available studies on system identification have been concentrated on the classical Hammerstein and Wiener models [10–12]. In this paper, the studied identification problem is of a general nature. On the one hand, the considered nonlinear system is a Hammerstein-Wiener structure comprising nonlinear, linear, and nonlinear blocks connected in series (Figure 1). On the other hand, the input nonlinearity is a discontinuous function with a series of discontinuous linear segments, as shown in Figure 2. Note that Wiener and Hammerstein systems can be viewed as specific examples of the suggested nonlinear model. The practical benefits of Hammerstein-Wiener models are revealed in various applications [13–15]. The nonlinear systems possessing discontinuous nonlinearities are of great importance in practical applications [8]. It should be noted that the discontinuity effect may lead to the series expansion reaching a highly complicated task [16]. For example, Figure 3 demonstrates that approximating the discontinuous nonlinearity resulting from the use of a high degree m of series expansion is challenging. Ref. [17] considered a Hammerstein system to solve the identification problem of hard nonlinearity (of known structure). In [8], a discontinuous piecewise linear function is considered in the case of the Wiener model.

The identification of the Hammerstein-Wiener system is rarely considered, and most available methods are focused on Hammerstein and Wiener systems [3, 18, 19]. In [20], the identification can be conducted

* Corresponding author (email: fatimaezzahraelmansouri95@gmail.com)

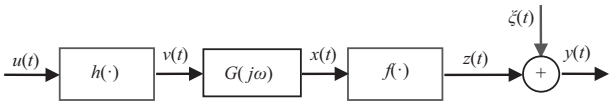

Figure 1 Hammerstein-Wiener system having discontinuous nonlinearity in the input.

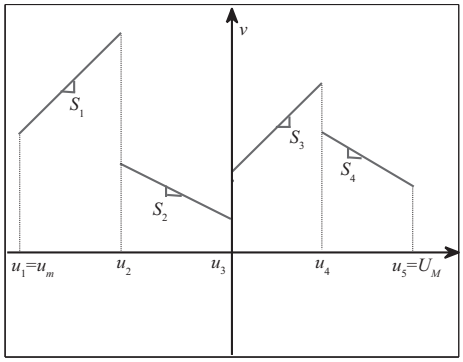

Figure 2 Example of discontinuous nonlinearities.

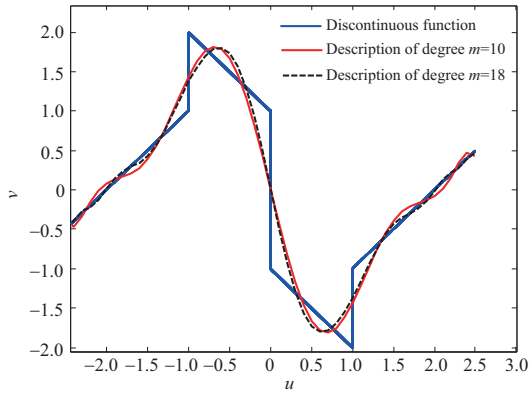

Figure 3 (Color online) Approximation of an example of a discontinuous function using polynomial expansion.

using a maximum-likelihood-based method, wherein the derivatives of the system nonlinearities, with respect to their parameter vectors, are assumed to have finite values. In [21–23], the identification of the Hammerstein-Wiener model has been achieved using frequency domain techniques. In [24], a solution is proposed that employs refined instrumental variables under the assumption of monotonic functions. In [25], an identification approach is proposed based on over-parametrization solutions. In [26], an identification method is developed based on the stochastic gradient descent algorithm. In [27], an iterative identification method is proposed. In [28], the identification takes into account continuous input nonlinearity. In [29], the linear time-invariant plant is assumed to be known. As a result, the majority of available research focused on the identification of the Hammerstein-Wiener model by considering a continuous input nonlinearity and/or an invertible output nonlinearity.

Main contributions and outline of the paper. The identification problem is addressed in this study using a Hammerstein-Wiener structure with discontinuous input nonlinearities and output nonlinearities that are not always invertible. The linear dynamical block can either be parametric or nonparametric. Unlike prior efforts that considered specific excitations and other assumptions, the suggested identification approach is based on simple (sine) excitations [30,31]. According to this, the identification is simple to implement. Finally, keep in mind that the input nonlinearity might have a variety of complex effects, e.g., saturation and/or dead zone. The outline of the remaining part of this paper is as follows: Section 2 states the identification difficulty. Section 2 begins with an explanation of the system and its assumptions. This section next discusses the uniqueness problem of model parameterization. Section 3 formally describes the nonlinear system identification approach. The identification of the output nonlinearity is addressed in Subsection 3.1. The identification of linear blocks is detailed in Subsection 3.3. The identification algorithm of the input nonlinearity is established. The performance of the suggested identification approach is shown in Section 4. Finally, the conclusion is given in Section 5.

Main notations used throughout the paper are as follows.

- $G(j\omega)$: transfer function of the linear block and $g(t)$ its impulse response.
- $\xi(t)$: a noise signal of expectation $E(\xi(t)) = 0$ and variance $\sigma^2 < \infty$.
- $*$: the convolution product.
- TL$(\cdot)$: the Laplace transform.
- $h(\cdot)$: input nonlinearity having l discontinuous segments of parameters (S_i, D_i) and $\bar{i} \in \{1, \ldots, l\}$ any segment.
- $f(\cdot)$: the output nonlinearity of parameter vector $\theta = (a_1, \hat{a}, a_n)^{\mathrm{T}}$.
- BIBO: bounded-input, bounded-output.
- $\omega_p; p = \{1, \ldots, l\}$: set of frequencies arbitrarily chosen by the designer.
- w.p.1: with probability 1.

- $\{(r_\lambda(t), y(t))\}$: curve composed of the set of points $\{(r_\lambda(t), y(t))\}$ over one period, in steady state.
- K: any integer such that KT is greater than the system response time.
- $(\hat{\cdot})$: the estimate value.

2 Identification problem formulation

2.1 System description and assumptions

In this study, the identification challenge of the Hammerstein-Wiener model (Figure 1) is dealt with. Then, this system is analytically designated by

$$v(t) = h(u(t)), \tag{1}$$

$$x(t) = g(t) * v(t), \tag{2}$$

$$z(t) = f(x(t)) = \sum_{k=1}^{n} a_k x^k, \tag{3}$$

$$y(t) = z(t) + \xi(t) = \sum_{k=1}^{n} a_k x^k + \xi(t), \tag{4}$$

where $G(j\omega) = \mathrm{TL}(g(t))$. Currently, the input block $h(\cdot)$ comprises a set of limited discontinuous linear segments. Consequently, this nonlinearity can have a dead zone, saturation, and other properties. The linear block $G(j\omega)$ can be parametric or not and is permitted to be of unknown structure. Only the input $u(t)$ and output $y(t)$ are accessible to measurements. As is demonstrated by Figure 2, the working interval $[U_{\min}, U_{\max}]$ can be decomposed into l subintervals:

$$[U_{\min}, U_{\max}] = [U_1, U_2] \cup [U_2, U_3] \cup [U_n, U_{n+1}], \tag{5}$$

where the inner signals $v(t)$ and $u(t)$ are linked by a linear function within any subinterval $[U_i, U_{i+1}]$, $i = 1, \ldots, l$,

$$v(t) = S_i u(t) + D_i. \tag{6}$$

The intervals border u_i, for $i = 2, \ldots, l$, are not previously known. Let us define the functions:

$$h_i\big(u(t)\big) = \begin{cases} S_i u(t) + D_i, & \text{for } i = 1, \ldots, l, \\ 0, & \text{for } i = 0. \end{cases} \tag{7}$$

We present the following switch signal $\sigma(\cdot)$:

$$\sigma\big(u(t)\big) = \begin{cases} 1, & \text{if } u \geqslant 0, \\ 0, & \text{else.} \end{cases} \tag{8}$$

By combining (6)–(8), the inner signal $v(t)$ can be expressed as follows:

$$v(t) = \sum_{i=1}^{l} [h_i(u(t)) - h_{\text{i-1}}(u(t))]\sigma(u(t) - u_i). \tag{9}$$

The studied Hammerstein-Wiener system (Figure 1) satisfies the following assumptions:

(A1) At least one segment is of the nonzero slope; i.e., there is $i \in \{1, \ldots, l\}$ such that $S_i \neq 0$.

(A2) The linear block is BIBO stable with nonzero static gain ($G(0) \neq 0$).

(A3) The nonlinearity $f(\cdot)$ is a polynomial function satisfying $f^{-1}(0) = 0$.

(A4) The noise $\xi(t)$ is any ergodic zero-mean process independent of the input.

Aside from assumptions (A1)–(A4), the nonlinear system of Figure 1 can be arbitrary. Moreover, the nonlinearity $f(\cdot)$ can be noninvertible for $x \neq 0$.

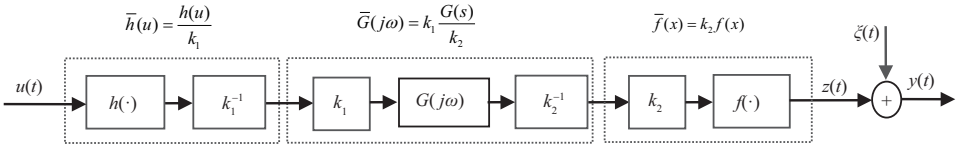

Figure 4 The generalized Hammerstein-Wiener system to be identified.

2.2 Problem of non-uniqueness of solution

The identification problem of the series connection of linear and nonlinear blocks does not possess a unique solution [1,21]. For instance, this identification problem (Figure 1) is of nonunique solution. Specifically, if the set of blocks $(h(u), G(j\omega), f(x))$ is a solution, then any model $(h(u)/k_1, k_1G(j\omega)/k_2, f(k_2x))$ is also solution for any nonzero scalars k_1 and k_2. For convenience, the generalized Hammerstein-Wiener model $(\bar{h}(u), \bar{G}(j\omega), \bar{f}(u))$ to be identified is provided by Figure 4, where

$$\bar{h}(u) = h(u)/k_1,\ \bar{G}(j\omega) = k_1G(s)/k_2,\ \bar{f}(x) = f(k_2x).$$

The current problem involves the choice of scalars k_1 and k_2 (Figure 4) for the uniqueness of solutions.

It is observed that a judicious choice of k_1 and k_2 can be conducted as

$$k_1 = S_{\bar{i}},\ k_2 = S_{\bar{i}}|G(j\omega_1)|, \tag{10}$$

where $\bar{i} \in \{1, \ldots, l\}$ is an arbitrarily segment of the nonlinearity $h(\cdot)$. Remarkably, the chosen frequency in (10) is not necessarily ω_1; it can be any arbitrary frequency from the set $\omega_1, \hat{a}, \omega_L$. The system to be identified will remain noted to avoid multiple notations $(h(\cdot), G(j\omega), f(\cdot))$. Accordingly, Eq. (10) implies that the system to be determined satisfies the following properties:

$$S_{\bar{i}} = 1,\ |G(j\omega_1)| = 1. \tag{11}$$

Definition 1. A signal $z(t)$ satisfies the T-periodicity property if it is periodic of period T, i.e., $z(t+T) = z(t)$, for any time t.

Lemma 1. Consider that the nonlinear system of Figure 1 is excited any sine signal $u(t) = U\cos(\omega t)$. Subsequently, the undisturbed output $z(t)$ satisfies the T-periodicity property, where $T = 2\pi/\omega$. Additionally, there exists a time $t_1 > 0$ such that the curve C is composed of the set of points:

$$C = (u(t), z(t)),\ t \in [t_1,\ t_1 + T)$$

which is a closed curve, referred to as the locus.

Proof. The considered nonlinear system introduces no bifurcations or chaos problems [21]. Moreover, the linear block is BIBO stable (A2). Subsequently, for any (T-periodic) sine input $u(t)$, the inner signals $v(t), x(t)$, and $z(t)$ are also T-periodic in steady state, but not necessarily sine wave. This implies that there exists a time t_1 such that, for any $t > t_1$, the signal $z(t)$ is periodic of the same period T as $u(t)$, where t_1 is greater than the system rise time. Finally, one immediately obtains the following:

$$(u(t+T), z(t+T)) = (u(t), z(t)),\ \text{for any } t > t_1.$$

This result suggests that C is a closed curve. This completes the proof of Lemma 1.

Definition 2. A curve C, described by the set of points $C = (u(t), z(t)), t \geqslant 0$, is known as static if and only if, for a T-periodic signal $u(t)$, one has $(u(t), z(t)) = (u(t+T), z(t+T))$, and the area encircled by C over one period (i.e., $(u(t), z(t)), t \in [t_1,\ t_1 + T)$ for any t_1 is zero).

3 Identification scheme

In this section, we attempt to develop an identification scheme to obtain the following:

- The estimate of the input nonlinearity parameters (S_i, D_i), for $i = 1, \ldots, l$.
- The complex gain $G(j\omega)$ (i.e., the gain module estimate) $|G(j\omega)|$ and the phase estimate $\hat{\varphi}(\omega)$ for any given set of frequencies $\omega \in (\omega_1, \ldots, \omega_L)$ (arbitrarily chosen).
- The estimate $(\hat{a_1}, \ldots, \hat{a_n})^{\mathrm{T}}$ of the output nonlinearity parameters.

3.1 Output nonlinearity identification (ONI)

Firstly, the nonlinear system Figure 1 is being excited by the sine wave:

$$u(t) = u_0 + U\cos(\omega t) \ \text{ where } \omega \in (\omega_1, \ldots, \omega_L). \tag{12}$$

Let us consider the reference sine signal $r_\lambda(t)$ of the same frequency ω and amplitude U as the input $u(t)$:

$$r_\lambda(t) = U\cos(\omega t + \lambda), \tag{13}$$

where $\lambda \in [-\pi, 0)$. Then, let the curve $C_\lambda(\omega)$, determined by the set of points:

$$C_\lambda(\omega) = (r_\lambda(t), z(t)),\ t \in [KT, (K+1)T) \ \text{ with } T = \frac{2\pi}{\omega}, \tag{14}$$

where K is any integer such that KT is greater than the system response time. Accordingly, $C_\lambda(\omega_1)$ is a closed curve (locus) employing Lemma 1. An example of a locus $C_\lambda(\omega)$ that can be obtained, for $\lambda \neq \varphi(\omega)$ (modulo π), is given by Figure 5(a). When $u(t)$ moves on one single segment of $h(\cdot)$ of parameters (S_i, D_i), then it follows from (2), (3), and (13) ($r_\lambda(t)$ for $\lambda = \varphi(\omega)$) that

$$z(t) = f(X_i + S_i|G(j\omega)|r_{\varphi(\omega)}(t)), \tag{15a}$$

where

$$X_i = G(0)(S_i u_0 + D_i). \tag{15b}$$

It is observed from (14), (15a), and (A3) that if $S_i = 1$ and $|G(j\omega)| = 1$, the set of points $(r_{\varphi(\omega)}(t), z(t))$ describing the curve $C_{\varphi(\omega)}(\omega)$ corresponds to the output nonlinearity $f(\cdot)$ shifted by X_i from the original. Figure 5(b) shows an example of a static curve of $C_\lambda(\cdot)$ that can be obtained. This outcome is quite interesting, and it demonstrates that if $z(t)$ is accessible to measurement, then $f(X_i+x)$ can be estimated.

Remark 1. The output $y(t)$ is recorded for an interval $[0,\ NT)$, where N is any integer preferably of large value. Benefiting from the T-periodicity property of $z(t)$ and employing (4), an accurate estimate $\hat{z}(t)$ of $z(t)$ can be acquired using the following estimator:

$$\begin{cases} \hat{z}(t) = \frac{1}{N}\sum_{k=0}^{N-1} y(t+kT), & \text{for } t \in [0,\ T), \\ \hat{z}(t+KT) = \hat{z}(t), & \text{for } k = 1, 2, \ldots. \end{cases} \tag{16}$$

It follows (11), for any segment $\bar{i} \in \{1, \ldots, l\}$ and for $\omega = \omega_1$, Eqs. (15a) and (15b) can be rewritten as

$$z(t) = f(X_{\bar{i}} + r_{\varphi(\omega_1)}(t)), \tag{17a}$$

$$X_{\bar{i}} = G(0)(u_0 + D_{\bar{i}}). \tag{17b}$$

According to the result provided by (17a), the curve $C_\lambda(\omega_1)$ is static if and only if $\lambda = \varphi(\omega_1)$ (modulo π). Moreover, for $\lambda = \varphi(\omega_1)$ (modulo π), $C_\lambda(\omega_1)$ corresponds to $f(X_{\bar{i}} \pm r_{\varphi(\omega_1)}(t))$. These outcomes can be checked practically by plotting the curve $\Gamma_\lambda(\omega_1) = (r_\lambda(t), y(t))$. The curve $\Gamma_\lambda(\omega_1)$ is detected for different values of λ in $[\pi, 0)$. The phase estimate $\hat{\varphi}(\omega_1)$ is the value of λ, noted $\bar{\lambda}$, causing a static curve (up to noise) of $\Gamma_\lambda(\omega_1)$. Subsequently, an accurate estimate of $\varphi(\omega_1)$ can be yielded by plotting $\hat{C}_\lambda(\omega_1) = (r_\lambda(t), \hat{z}(t)), t \in [0,\ T)$, using (16), and checking the best value of $\bar{\lambda}$. Additionally, according to (17a), one immediately obtains $\hat{f}(X_{\bar{i}} + x) = \hat{C}_{\bar{\lambda}}(\omega_1)$. By combining this result with (A3), the offset of $X_{\bar{i}}$ can be easily estimated and $\hat{f}(x)$ is attained by shifting $\hat{C}_{\bar{\lambda}}(\omega_1)$ to the origin. Finally, employing (A3), the obtained parameter estimates of $f(\cdot)$ are maintained over the working interval.

Remark 2 (Hierarchical least-squares method)**.** The identification of the output nonlinearity $f(\cdot)$ can be performed using analytical or geometrical methods. In the analytical procedure, the hierarchical least-squares solution can be applied. Specifically, when the phase estimate $\hat{\varphi}(\omega_1)$ is known, the parameter vector θ of $f(\cdot)$ can be identified utilizing the classical least-squares method (LSM) and minimizing the error:

$$e^2(t) = \sum_{t=1}^{\mathrm{T}} \left(\hat{z}(t) - \sum_{k=0}^{n} a_k (\widehat{X}_{\bar{i}} + r_{\hat{\varphi}(\omega_1)}(t))^k \right)^2. \tag{18}$$

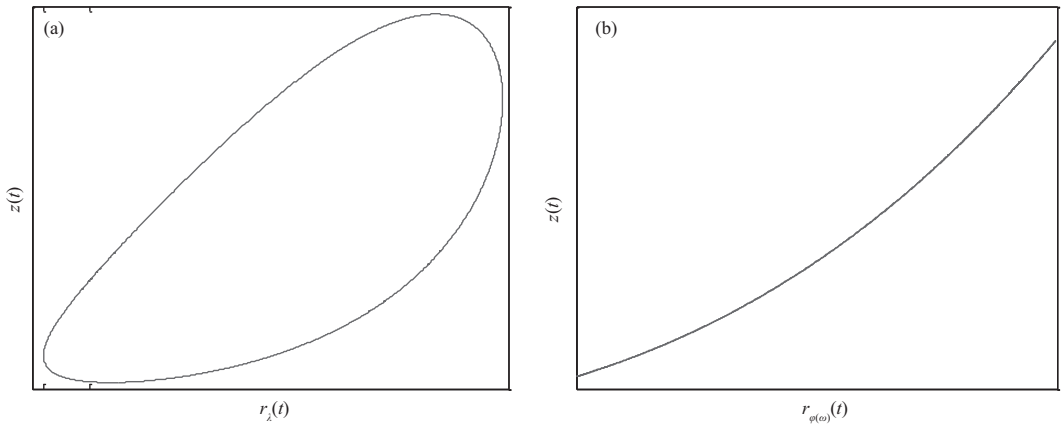

Figure 5 Example of (a) obtained closed curve (locus) of $C_\lambda(\cdot)$ and (b) obtained static curve of $C_\lambda(\cdot)$.

The primary challenge in the criteria (18) is that $\hat{\varphi}(\omega_1)$ is unknown at this stage. It follows that the classical LSM cannot directly be implemented to determine the parameter vector θ. To overcome this difficulty, a hierarchical least-squares solution can be proposed. Specifically, the classical least-squares solution using the criteria (18) can be established for any given value of $\lambda \in [-\pi, 0)$. Subsequently, by knowing the range of λ (i.e., $[-\pi, 0)$) and varying λ from $-\pi$ to 0, an accurate estimate of $\varphi(\omega_1)$ and θ can be yielded by repeating the LSM algorithm.

For convenience, the main steps in the ONI algorithm are summarized in Algorithm 1.

Algorithm 1 ONI algorithm

Initialization step. Set the amplitude U to any small value and select any frequency $\omega \in (\omega_1, \ldots, \omega_L)$; for instance, the frequency ω_1 is taken. Choose any value for $u_o \in [u_{\min}, u_{\max}]$ and any large integer N.

Step 1 (Setting of the offset u_o). Excite the system by (12) and consider the signal $r_\lambda(t)$ given by (13). Using the collected $y(t)$, plot the curve $\Gamma_\lambda(\omega_1) = (r_\lambda(t), y(t))$ over one period (in steady state). Check whether $\Gamma_\lambda(\omega_1)$ can become a static curve (up to noise) when λ varies in $[-\pi, 0)$. Else, the value of u_o can be adjusted.

Step 2 (Phase estimate $\hat{\varphi}(\omega_1)$). Using the collected $y(t)$ and the estimator (16), give the estimate $\hat{z}(t)$ and plot $\hat{C}_\lambda(\omega_1) = (r_\lambda(t), \hat{z}(t)) : t \in [0, 2\pi/\omega_1)$. Look for the value $\bar{\lambda}$ of $\lambda \in [-\pi, 0)$ leading to a static curve of $\hat{C}_\lambda(\omega_1)$. Subsequently, the estimate of $\varphi(\omega_1)$ is $\hat{\varphi}(\omega_1) = \bar{\lambda}$.

Step 3 (The nonlinearity estimate $\hat{f}(\cdot)$). Using (17a) and (17b), one has $\hat{f}(X_{\bar{i}} + x) = \hat{C}_{\bar{\lambda}}(\omega_1)$. Using (A3), determine $\hat{f}(\cdot)$ by translating $\hat{C}_{\bar{\lambda}}(\omega_1)$ to the origin and assume the estimate of $X_{\bar{i}}$.

Theorem 1. Consider the above identification problem. Then, one has the following convergences with probability 1 (w.p.1):

(1) The estimator (16) is consistent w.p.1, i.e., $\hat{z}(t) \xrightarrow[N\to\infty]{} z(t)$ (w.p.1).

(2) The output nonlinearity estimate $\hat{f}(\cdot)$ converges to the true nonlinearity $f(\cdot)$ w.p.1, i.e., $\hat{f}\ (\cdot) \xrightarrow[N\to\infty]{} f\,(\cdot)$.

Proof. (1) When the nonlinear system (1)–(4) is excited by a T-periodic signal, then the undisturbed output $z(t)$ satisfies the T-periodicity property, where $T = 2\pi/\omega$ is the period of $u(t)$. Accordingly, it follows (4) and (16), one immediately yields

$$\hat{z}(t) = z(t) + \frac{1}{N}\sum_{k=0}^{N-1} \xi(t + kT). \tag{19}$$

Recall that the extra-input $\xi(t)$ is ergodic zero-mean process, then,

$$\frac{1}{N}\sum_{k=0}^{N-1} \xi(t + kT) = \frac{1}{N}\sum_{t=0}^{N-1} \xi(t) \overset{N\to\infty}{\longrightarrow} 0. \tag{20}$$

Consequently, the proof of the first part can be attained by combining (19) and (20).

(2) The curve $C_\lambda(\omega) = (r_\lambda(t), z(t))$ is static if and only if $\lambda = \varphi(\omega)$ (modulo π). This result can be proven using the T-periodicity property (Definition 1) of $r_\lambda(t)$ and $z(t)$, where $T = 2\pi/\omega$, and comparing it with (17a) and (14). Additionally, using Lemma 1 the curve induced by $(r_\lambda(t), z(t))$ for $\lambda \neq \varphi(\omega)$ (modulo π) is a closed locus.

For $\lambda = \varphi(\omega)$ (modulo π), it is demonstrated that the locus $C_\lambda(\omega)$ becomes a static curve. Hence, using (17a)–(14) it is readily observed that $C_{(\pm\varphi(\omega))}(\omega) = (r_{\pm\varphi(\omega)}(t), z(t))$ corresponds to either $f(X_{\bar{i}} + x(t))$ or $f(X_{\bar{i}} - x(t))$. This implies that the estimate $\hat{f}(X_{\bar{i}} + x)$ corresponds to $C_{\bar{\lambda}}(\omega)$.

Specifically, the output nonlinearity estimate $\hat{f}(X_{\bar{i}} + x)$ corresponds to $f(X_{\bar{i}} + x(t))$ or to $f(X_{\bar{i}} - x(t))$. This uncertainty is not an issue because the sign "$-$" will be included in the scaling factor k_2 (see the non-uniqueness problem in Subsection 2.2).

Finally, using the first part of Theorem 1, one immediately obtains $\hat{f}(X_{\bar{i}} + x) = (r_{\bar{\lambda}}(t), \hat{z}(t)) \overset{N\to\infty}{\longrightarrow} f(X_{\bar{i}} + x)$. This completes the proof of Theorem 1.

3.2 Linear dynamic element identification (LDEI)

Currently, the considered linear element is not necessarily parametric. Knowing the phase $\varphi(\omega_1)$ and $|G(j\omega_1)| = 1$, using (11), the objective is to estimate $|G(j\omega)|$ and $\varphi(\omega)$ for any frequency $\omega_p \in (\omega_2, \ldots, \omega_L)$. Firstly, note that the phase estimate $\hat{\varphi}(\omega)$, for any ω, can be acquired using the same method used in the output nonlinearity identification (ONI) and by keeping the values of (U, u_o) constant. Hence, the estimate $\hat{\varphi}(\omega)$ is the value $\bar{\lambda}_p$ of λ causing a static curve of $C_\lambda(\omega)$. Then, it follows (15a); using the first property of (11), one obtains the following:

$$\hat{f}\left(X_{\bar{i}} + \left|\hat{G}(j\omega)\right| r_{\hat{\varphi}(\omega)}(t)\right) = \hat{C}_{\bar{\lambda}_p}(\omega). \tag{21}$$

$X_{\bar{i}}$ has already been identified in the ONI. Accordingly, by combining (21) and the assumption $f^{-1}(0) = 0$, one has, for $k = 1\hat{a}n$,

$$f\left(|G(j\omega)|x\right) = \sum_{k=1}^{n} \bar{a}_k(\omega) x^k = \sum_{k=1}^{n} a_k \left|G(j\omega)\right|^k x^k, \tag{22}$$

where $\bar{a}_k(\omega) = a_k(\omega)\left|G(j\omega)\right|^k, k \in 1, \ldots, n$. Then, the latter can be easily determined using only the available data acquisition. Consequently, the only unknown parameter in (22) is the gain $|G(j\omega)|$. Finally, the gain $|G(j\omega)|$ can be estimated using only one coefficient $\bar{a}_k(\omega)$ $(k \in (1, \hat{a}, n))$ of $f\left(|G(j\omega)|x\right)$.

Remark 3. To improve the identification accuracy of the gain $|G(j\omega)|$, for any frequency $\omega \in (\omega_1, \hat{a}, \omega_L)$, it is remarkable to benefit from all the estimates $\hat{\bar{a}}_k(\omega)$ of $\bar{a}_k(\omega)$, for $k = 1\hat{a}n$. Then, the following estimator of the gain $|G(j\omega)|$ is proposed:

$$\left|\hat{G}(j\omega)\right| = \frac{1}{n}\sum_{k=1}^{n}\left|\frac{\hat{\bar{a}}_k(\omega)}{\hat{a}_k}\right|^{1/k}. \tag{23}$$

Finally, the key steps corresponding to the LDEI algorithm are expressed in Algorithm 2.

Algorithm 2 LDEI algorithm

Initialization step. (U, u_o) of $u(t)$ in (12) is initialized by their values used in the ONI algorithm.
Step 1 Estimate of $G(s)$ **for** $\omega = \omega_1$**.** Using (11), one gets $|G(j\omega_1)| = 1$. It follows from Step 2 of the ONI algorithm that one has $\hat{\varphi}(\omega_1) = \bar{\lambda}$.
Step 2 (Data acquisition). For $\omega \in (\omega_2, \ldots, \omega_L)$, excite the system by (12). Using the collected $y(t)$ and (16), identify the estimate $\hat{z}(t)$. Plot $\hat{C}_\lambda(\omega) = (r_\lambda(t), \hat{z}(t)), t \in [0, 2\pi/\omega]$, where $r_\lambda(t)$ is given by (13).
Step 3 (Phase estimate $\hat{\varphi}(\omega)$**).** Search the value $\bar{\lambda}p$ of λ causing a static curve of $\hat{C}_\lambda(\omega)$, by varying λ of (13) in $[-\pi, 0)$. Then, one has the estimate $\hat{\varphi}(\omega) = \bar{\lambda}p$.
Step 4 (Gain estimate $|\hat{G}(j\omega)|$**).** One has $\hat{f}(X_{\bar{i}} + |\hat{G}(j\omega)| r_{\hat{\varphi}(\omega)}(t)) = \hat{C}_{\bar{\lambda}_p}(\omega)$ (using 21), where $X_{\bar{i}}$ is identified in Step 3 of the ONI algorithm. Using (A3), (21), and (22), the gain estimate is $|\hat{G}(j\omega)| = \frac{1}{n}\sum_{k=1}^{n}|\frac{\hat{\bar{a}}_k(\omega)}{\hat{a}_k}|^{1/k}$. Then, take another frequency $\omega \in (\omega_1, \ldots, \omega_L)$ and go to Step 2 or the end of the algorithm.

Remark 4. The gain and the phase of the linear block, for $\omega = \omega_1$, are determined in the first stage (Subsection 3.1). Besides, the identification of linear block $|G(j\omega)|$, for the set of frequencies $(\omega_2, \hat{a}, \omega_L)$, can be conducted using only the obtained results from the ONI algorithm and phase estimates, i.e., without requiring any other experiment.

Theorem 2. Consider the LDEI algorithm. Then, $\hat{G}(j\omega)$ converges to $G(j\omega)$, for any ω, w.p.1, i.e., $\hat{\varphi}(\omega) \xrightarrow[N\to\infty]{} \varphi(\omega)$ and $|\hat{G}(j\omega)| \xrightarrow[N\to\infty]{} |G(j\omega)|$.

Proof. Firstly, suppose that the parameters determined in the ONI algorithm are accurately identified and can be replaced by their true values, i.e., $(\hat{\theta}, \hat{X}_{\bar{i}})$ by $(\theta, X_{\bar{i}})$. Employing the ONI algorithm and

Theorem 1, it is demonstrated that $C_\lambda(\omega) = (r_\lambda(t), z(t))$ is static if and only if $\lambda = \varphi(\omega)$ (modulo π) and $\hat{f}(\cdot) \xrightarrow[N\to\infty]{} f(\cdot)$. This result is valid for any frequency ω. Then, it is easily seen that

$$\hat{z}(t) = z(t) + \frac{1}{N}\sum_{k=0}^{N-1} \xi(t+kT) \xrightarrow[N\to\infty]{} z(t).$$

Using (17a), one gets for any given frequency ω

$$\hat{z}(t) = \sum_{k=0}^{n} a_k \left(X_{\bar{i}} + |\hat{G}(j\omega)| r_{\hat{\varphi}(\omega)}(t)\right)^k \xrightarrow[N\to\infty]{} z(t) = \sum_{k=0}^{n} a_k \left(X_{\bar{i}} + |G(j\omega)| r_{\varphi(\omega)}(t)\right)^k.$$

This result is equivalent to (for any time t)

$$\hat{z}(t) - z(t) = \sum_{k=0}^{n} a_k \left[\left(X_{\bar{i}} + |\hat{G}(j\omega)| r_{\hat{\varphi}(\omega)}(t)\right)^k - \left(X_{\bar{i}} + |G(j\omega)| r_{\varphi(\omega)}(t)\right)^k\right] \xrightarrow[N\to\infty]{} 0,$$

which causes the following convergences: $(|\hat{G}(j\omega)|, \hat{\varphi}(\omega)) \xrightarrow[N\to\infty]{} (|G(j\omega)|, \varphi(\omega))$.

3.3 Input nonlinearity identification (INI)

Currently, the nonlinear system is excited by the same input (12) for $\omega = \omega_1$ and U is set to any small value. Firstly, using the properties (11), the gain modulus $|G(j\omega)|$ for $\omega = \omega_1$ and the slope of the segment $\bar{i}$ are exactly determined, i.e., $|G(j\omega_1)| = 1$ and $S_{\bar{i}}$. Then, the static gain $G(0)$ and the parameter $D_{\bar{i}}$ can be obtained using the estimate of $X_{\bar{i}}$ given by (17b) for two values of u_o.

The objective is to identify the parameters (S_i, D_i) of any segment i and its boundaries (of the intervals $[u_i, u_{i+1}]$) for $i = 1, \ldots, l$. For convenience, let us consider the reference wave $r_\lambda(t)$ defined by (13), where $\omega = \omega_1$ and $\lambda = \bar{\lambda} = \hat{\varphi}(\omega_1)$,

$$r_\lambda(t) = U\cos(\omega_1 t + \bar{\lambda}). \tag{24}$$

Firstly, to regulate the parameters of the first segment ($i = 1$), u_o in (12) is initialized with the value $u_{\min} + U$. In the sequel (during the INI stage), the parameters of the reference $r_\lambda(t)$ will be maintained. Let t_1 denote any time taken in a steady state (larger than the system rise time). As a result, it is readily observed that if the curve defined by

$$C_{\bar{\lambda}}(\omega_1) = (r_{\bar{\lambda}}(t), z(t)), \text{ for } t \in \left[t_1, t_1 + \frac{2\pi}{\omega_1}\right] \tag{25}$$

is static. This suggests that the input $u(t)$ moves on a single segment of $h(\cdot)$. When the curve estimate $\hat{C}_{\bar{\lambda}}(\omega_1)$, established by replacing $z(t)$ by its estimate $\hat{z}(t)$, is not static, the amplitude U should be decreased. Using (11)–(15a), the estimate of $f(X_1 + S_1 r_{\bar{\lambda}}(t))$ is provided as

$$\hat{f}(\hat{X}_1 + \hat{S}_1 r_{\bar{\lambda}}(t)) = \hat{C}_{\bar{\lambda}}(\omega_1), \tag{26a}$$

where $X_1 = G(0)(S_1 u_o + D_1)$ and its estimate is

$$\hat{X}_1 = \hat{G}(0)(\hat{S}_1 u_o + \hat{D}_1). \tag{26b}$$

This result allows S_1 and X_1 to be obtained using the estimate $\hat{f}(\cdot)$ and $f^{-1}(0) = 0$. Afterward, $\hat{D}_1$ can be acquired using (26b) and $\hat{X}_1$. Then, increasing u_o and allowing u_0^* represent the first value of u_o results in $\hat{C}_{\bar{\lambda}}(\omega_1)$ becoming nonstatic. Finally, the estimate $\hat{u}_2$ of u_2 is given as follows:

$$\hat{u}_2 = u_0^* + U. \tag{27}$$

The same experiment is repeated by initializing u_o with the value $\hat{u}_2 + U$. To estimate the parameters of the second segment ($i = 2$). The primary steps involved in INI are summarized in Algorithm 3.

Algorithm 3 INI algorithm

Initialization step. In $r_\lambda(t)$ of (24), set $\omega_p = \omega_1$, $i = 1$, $\lambda = \bar{\lambda} = \hat{\varphi}(\omega_1)$ and U is fixed to any small value. Collect $r_\lambda(t)$ for $t \in [0, 2\pi/\omega_1]$. In (12), set the offset $u_o = u_{\min} + U$.
Step 1. Data acquisition. Excite the system by (12). Utilizing the collected $y(t)$, construct $\hat{z}(t)$ by (16).
Step 2. Construct the curve estimate $\hat{C}_{\bar{\lambda}}(\omega_1) = (r_\lambda(t), \hat{z}(t)), t \in [0, 2\pi/\omega_1)$. If $\hat{C}_{\bar{\lambda}}(\omega_1)$ is nonstatic, reduce the amplitude U and go to Step 1. Otherwise, go to Step 3.
Step 3. Using $\hat{f}(\cdot)$ provided by the ONI algorithm and $f^{(-1)}(0) = 0$, calculate $\hat{X}_i$ and $\hat{S}_i$ using (26a). Using (26b) and the estimate $\hat{X}_i$, determine $\hat{D}_i$.
Step 4. u_o is gradually increased, by checking if $u_o + U = u_{\max}$ and $\hat{C}_{\bar{\lambda}}(\omega_1)$ is still static; then go to Step 6. Otherwise, record u_0^* the first value of u_o inducing a nonstatic curve of $\hat{C}_{\bar{\lambda}}(\omega_1)$, increment $(i = i + 1)$, and take the estimate $\hat{u}_i = u_0^* + U$.
Step 5. Update the offset u_o of (12) with $u_o = \hat{u}_i + U$ and go to Step 1.
Step 6. End step. Take the number of discontinuous segments (of $h(\cdot)$)$l = i$ and set $[u_{\min}, u_{\max}] = [u_1, \hat{u}_2] \cup \cdots \cup [\hat{u}_l, u_{\max}]$. Give the estimates $(\hat{S}_i, \hat{D}_i)$ $(i = 1, \ldots, l)$ of $h_i(\cdot)$ obtained in Step 3.

Theorem 3. Consider the INI algorithm. Then, one has the following convergences (for $i = 1, \ldots, l$) w.p.1:

(1) The estimates of interval boundaries $\hat{u}_i \xrightarrow[N\to\infty]{} u_i$.

(2) The segment parameters $(\hat{S}_i, \hat{D}_i)$ converge to (S_i, D_i), i.e., $\hat{h}(\cdot) \xrightarrow[N\to\infty]{} h(\cdot)$.

Proof. (1) Firstly, assume that the parameters determined by the LDEI and INI algorithms are correctly determined, e.g., $\hat{f}(\cdot) \xrightarrow[N\to\infty]{} f(\cdot)$ and $\hat{\varphi}(\omega_1) \xrightarrow[N\to\infty]{} \varphi(\omega)$. Suppose that there exists $\bar{u} \in \mathbb{R}^+$ such that when $N \to \infty$, $\hat{u}_i \to u_i + \bar{u}, i \in \{1, \ldots, l\}$, i.e., the input spans two segments of $h(\cdot)$ (step 4 of Algorithm 3). This implies that there exists a time $t_i > 0$ during the steady state such that

$$v(t) = \begin{cases} h_i(u(t)) = S_i u(t) + D_i, & \text{for } t \in [KT, KT + t_i), \\ h_{i+1}(u(t)) = S_{i+1} u(t) + D_{i+1}, & \text{for } t \in [KT + t_i, (K+1)T). \end{cases} \tag{28}$$

It is evident that the signal $v(t)$ is periodic; however, it does not appear to be a sine signal $(h_i(\cdot) \neq h_{i+1}(\cdot))$. Specifically, $v(t)$ is the sum of sine signals:

$$u(t) = \sum_{k=0}^{\infty} V_k \cos(k\omega_1 t + \psi_k). \tag{29}$$

Then, the inner signal $x(t)$ can be written as

$$x(t) = \sum_{k=0}^{\infty} V_k |G(jk\omega_1)| \cos(k\omega_1 t + \psi_k + \varphi(k\omega_1)). \tag{30}$$

The latter verifies that $x(t)$ is not a linear function based on $u(t)$, i.e.,

$$z(t) \neq f(X_1 + S_1 r_{\varphi(\omega_1)}(t)).$$

Accordingly, $C_{\varphi(\omega_1)}(\omega_1)$ is a closed curve and cannot boil down to a static curve. This completes the first part of the theorem.

(2) At this stage, suppose that $u(t)$ spans only one segment of $h(\cdot)$ ($C_{\varphi(\omega_1)}(\omega_1)$ is static). Utilizing Theorems 1 and 2, one gets for time any t and any fixed (S_i, D_i)

$$\hat{z}(t) = \sum_{k=0}^{n} a_k (\hat{X}_i + \hat{S}_i r_{\hat{\varphi}(\omega)}(t))^k \underset{N\to\infty}{\longrightarrow} z(t) = \sum_{k=0}^{n} a_k (X_i + S_i r_{\varphi(\omega)}(t))^k. \tag{31}$$

These outcomes immediately cause the convergences: $\hat{S}_i \xrightarrow[N\to\infty]{} S_i$ and $\hat{X}_i \xrightarrow[N\to\infty]{} X_i$ where $X_i = G(0)(\hat{S}_1 u_o + \hat{D}_1)$. Finally, the convergences of part 2 can be inferred. This completes the proof of Theorem 3.

4 Simulation

This section demonstrates the validation test of the current research. The input nonlinearity of the system (Figure 1) is a discontinuous function comprising four segments (Figure 6). The transfer function

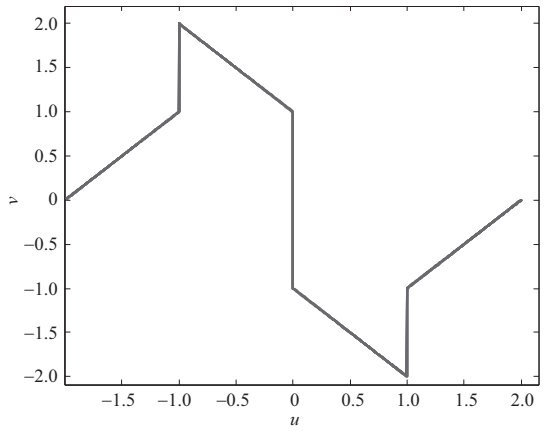

Figure 6 The nonlinearity $h(\cdot)$ used in simulation.

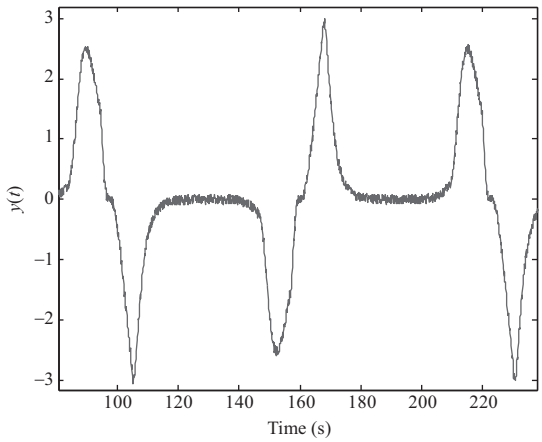

Figure 7 Example of obtained results of $y(t)$ when $u(t)$ crosses at least two segments.

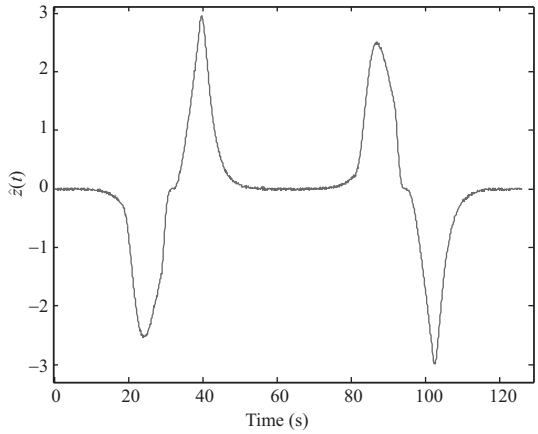

Figure 8 The filtered output $\hat{z}(t)$ for $U = 2$ and $\omega = \omega_1 = 0.05$.

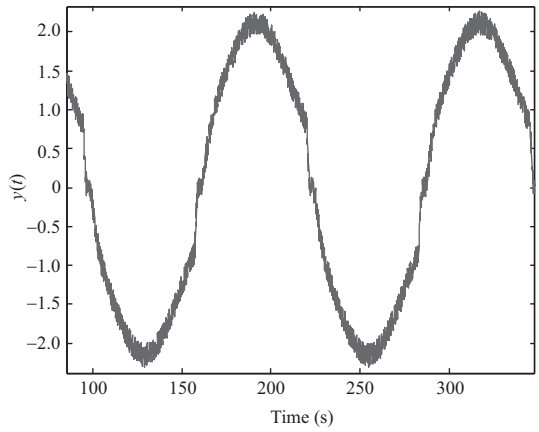

Figure 9 The output $y(t)$ for $U = 0.5$, $u_o = 0$, and $\omega = \omega_1 = 0.05$.

of the linear block is provided as follows:

$$G(s) = 0.3/(s + 0.7)(s + 0.5). \tag{32}$$

The output nonlinearity $f(\cdot)$ is chosen as polynomial type and is given by

$$f(x) = \sum_{k=0}^{n} a_k x^k = x^3 - 0.01x^2 + 0.02x, \tag{33}$$

where it satisfies $f^{(-1)}(0) = 0$ and the working interval is set to $[-2, 2]$. The noise $\xi(t)$ is featured by the properties $E(\xi(t)) = 0$ and $\sigma^2 = 0.15$.

Firstly, following the ONI algorithm, the system of Figure 1 is excited by the wave (12). For instance, the obtained output $y(t)$ for $U = 2$, $u_o = 0$, and $\omega_1 = 0.05$ rd/s is plotted in Figure 7.

This outcome means that $u(t)$ runs through at least two segments of $h(\cdot)$. This remark can be observed from the filtered output $\hat{z}(t)$, over one period, given by Figure 8.

The last experiment is repeated for other values of U; for instance, the obtained system output $y(t)$ for $U = 0.5$ is represented by Figure 9. For convenience, the filtered output $\hat{z}(t)$ employing the estimator (16) is plotted in Figure 10. Let us consider the frequency satisfying the property (10) and (11) is $\omega_1 = 0.05$ rd/s.

The obtained curve $\hat{C}_\lambda(\omega_1) = (r_\lambda(t), \hat{z}(t))$ for $\lambda = -1.5$ rd is given by Figure 11. It is seen that $\hat{C}_\lambda(\omega_1)$ tends to a closed curve, which verifies the results of Lemma 1. Then, by plotting $\hat{C}_\lambda(\omega_1)$ for various

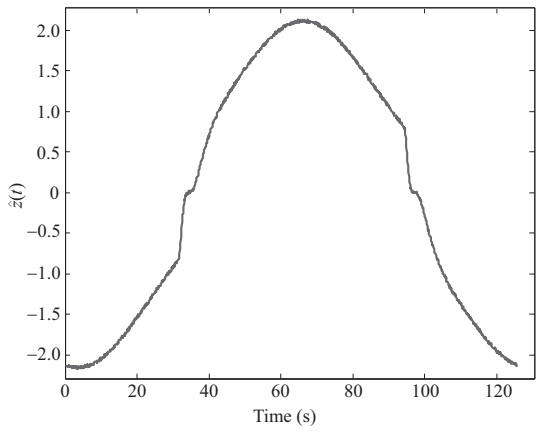

Figure 10 The filtered output $\hat{z}(t)$ for $U = 0.5$, $u_o = 0$, and $\omega = \omega_1 = 0.05$ rd/s.

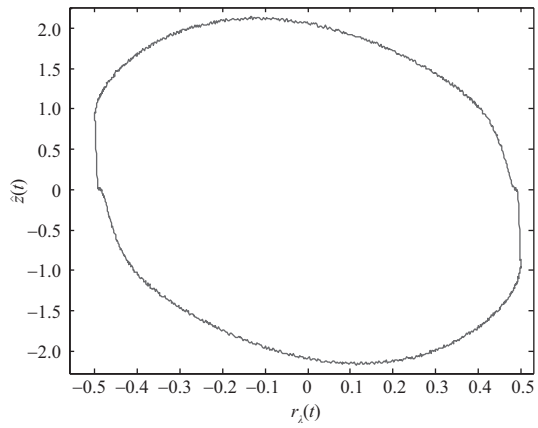

Figure 11 The curve $\hat{C}_\lambda(\omega_1)$ for an arbitrary value of λ.

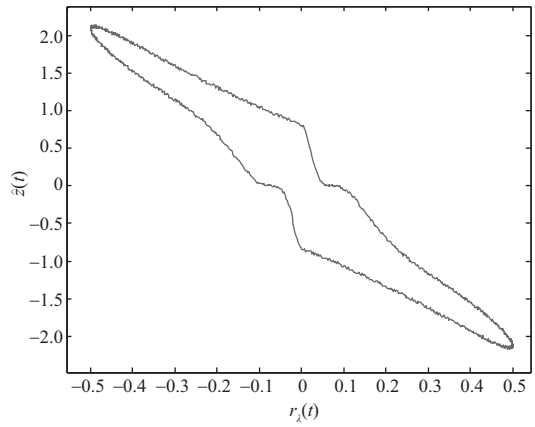

Figure 12 Locus $\hat{C}_\lambda(\omega_1)$ for $\lambda = -0.2$ rd.

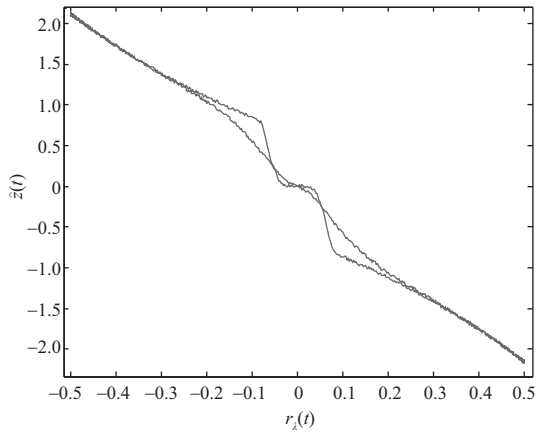

Figure 13 Curve $\hat{C}_\lambda(\omega_1)$ for $\lambda = -0.18$ rd.

values of λ in $[-\pi, 0)$ while keeping U and u_o constant, it is indicated that the area enclosed by $\hat{C}_\lambda(\omega_1)$ decreases for $\lambda \in [-0.1, -0.2]$, e.g., Figures 12 and 13. give $\hat{C}_\lambda(\omega_1)$ for $\lambda = -0.2$ rd and $\lambda = -0.18$ rd, respectively. However, $\hat{C}_\lambda(\omega_1)$ fails to converge to a static curve. For instance, Figure 13 demonstrates $\hat{C}_\lambda(\omega_1)$ when its area is minimized.

Accordingly, this outcome verifies that $u(t)$ crosses more than one segment of the nonlinearity $h(\cdot)$. Then, the value of u_o should be adjusted; e.g., for $u_o = 0.5$, the obtained output $y(t)$ is depicted by Figure 14. The filtered version $\hat{z}(t)$ is provided by Figure 15. For example, $\hat{C}_\lambda(\omega_1)$ is shown by Figure 16 for $\lambda = -1.74$ rd. This curve is not static, which implies that $\lambda \neq \varphi(\omega_1) \pm k\pi$, $k = 1, 2, \ldots$.

The curve $\hat{C}_\lambda(\omega_1)$ is plotted for different values of λ in $[-\pi, 0)$ until a static curve is observed. Hence, it is observed that the area enclosed by $\hat{C}_\lambda(\omega_1)$ starts to decrease when λ increases. For example, the obtained $\hat{C}_\lambda(\omega_1)$ for $\lambda = -0.52$ rd is demonstrated by Figure 17.

For $\lambda = -0.175$ rd, $\hat{C}_\lambda(\omega_1)$ almost becomes static, as demonstrated by Figure 18. This denotes that the phase estimate $\varphi(\omega_1) = \bar{\lambda} \approx -0.175$ rd and the static curve $\hat{C}_{\bar{\lambda}}(\omega_1)$ corresponds to the nonlinearity estimate $\hat{f}(X_{\bar{i}} + x)$. The latter can be employed to identify $X_{\bar{i}}$ in Figure 19.

For convenience, for two values of u_o ($u_{o1} = 0.5$) and ($u_{o2} = 0.25$), while $U = 0.25$, the nonlinearities $\hat{f}(X_{i1} + x)$ and $\hat{f}(X_{i2} + x)$ corresponding to u_{o1} and u_{o2}, respectively, can be yielded. Then, the estimates of $D_{\bar{i}}$ and $G(0)$ can be easily identified using X_{i1} and X_{i2}.

The identification of linear block for other frequencies $(\omega_2, \omega_3, \hat{a})$ is performed by repeating the same experiment. For example, the output $y(t)$ and $\hat{z}(t)$ for $\omega_2 = 0.1$ rd/s are plotted in Figures 20(a) and (b), respectively. Then, the curve $\hat{C}_\lambda(\omega_2)$ is plotted for various values of $\lambda \in [-\pi, 0)$; e.g., for $\lambda = -0.04$ rd, the obtained $\hat{C}_\lambda(\omega_2)$ is given by Figure 21(a). This result shows that $\hat{C}_\lambda(\omega_2)$ is not static, which denotes

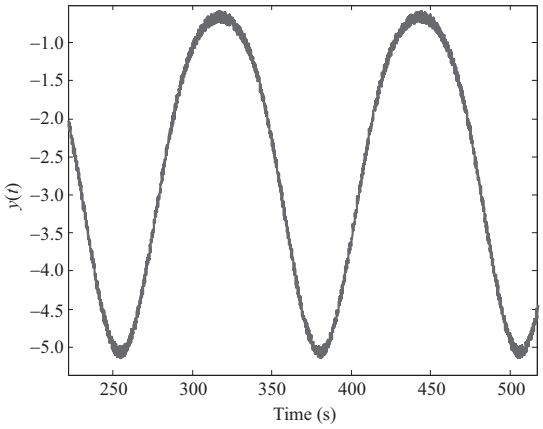

Figure 14 Output $y(t)$ for $U = 0.5$, $u_o = 0.5$, and $\omega = \omega_1 = 0.05$ rd/s.

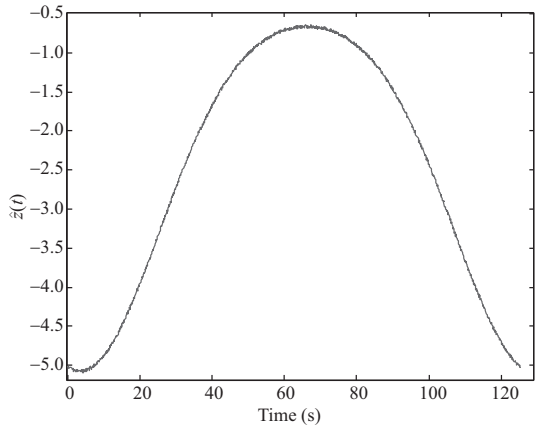

Figure 15 Filtered output $\hat{z}(t)$ for $\omega = \omega_1$ and $U = u_o = 0.5$.

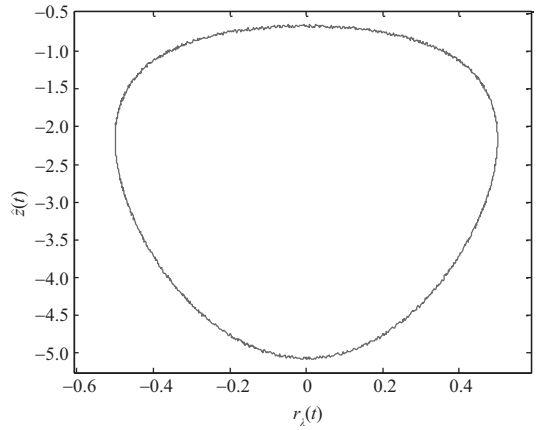

Figure 16 Curve $\hat{C}_\lambda(\omega_1)$ for an arbitrary value of λ.

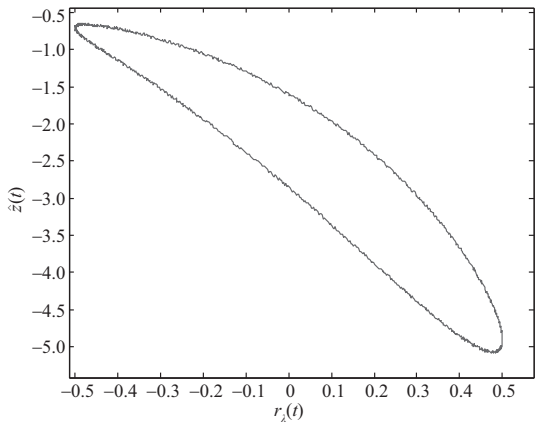

Figure 17 Curve $\hat{C}_\lambda(\omega_1)$ for $\lambda = -0.52$ rd.

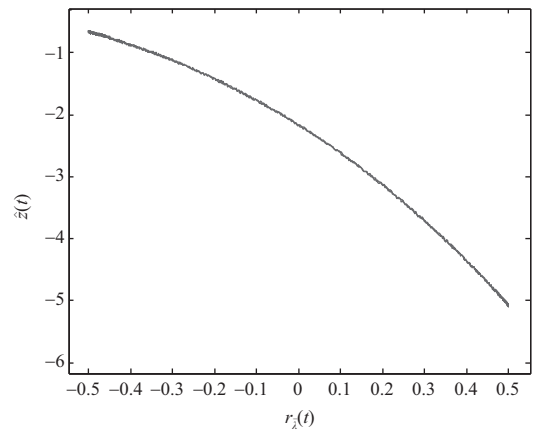

Figure 18 Curve $\hat{C}_\lambda(\omega_1)$ for $\lambda \approx \varphi(\hat{\omega})$ (modulo π).

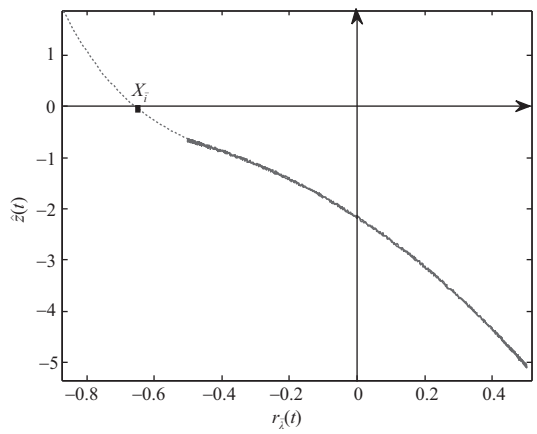

Figure 19 Determination of $X_{\bar{i}}$ using $\hat{f}(X_{\bar{i}} + x) = \hat{C}_{\bar{\lambda}}(\omega_1)$.

that $\lambda \neq \varphi(\omega_2)$ (modulo π).

The obtained estimate $\hat{\varphi}(\omega_2)$ is $\bar{\lambda}_2 \approx -0.34$ rd. Regarding this, the corresponding curve $\hat{C}_{\bar{\lambda}_2}(\omega_2)$ is provided by Figure 21(b). For convenience, the obtained phase estimates with their true value for $\omega_p \in (0.05, 0.1, 0.5)$ rd/s are summarized in Table 1.

Firstly, by Eq. (11) one has $|G(j\omega_1)| = 1$. Then, for any other frequency $\omega \neq \omega_1$, using the obtained

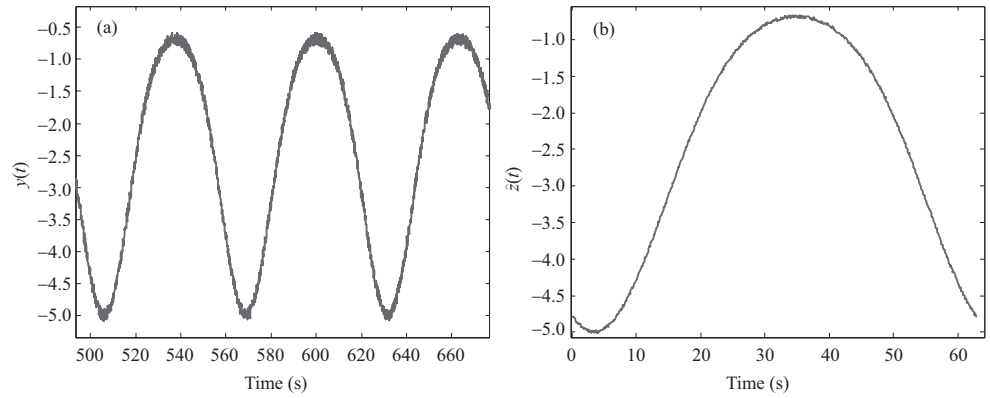

Figure 20 (a) Output $y(t)$ for $U = 0.5$, $u_o = 0.5$, and $\omega_2 = 0.1$ rd/s; (b) filtered output $\hat{z}(t)$ for $U = 0.5$, $u_o = 0.5$, and $\omega_2 = 0.1$ rd/s.

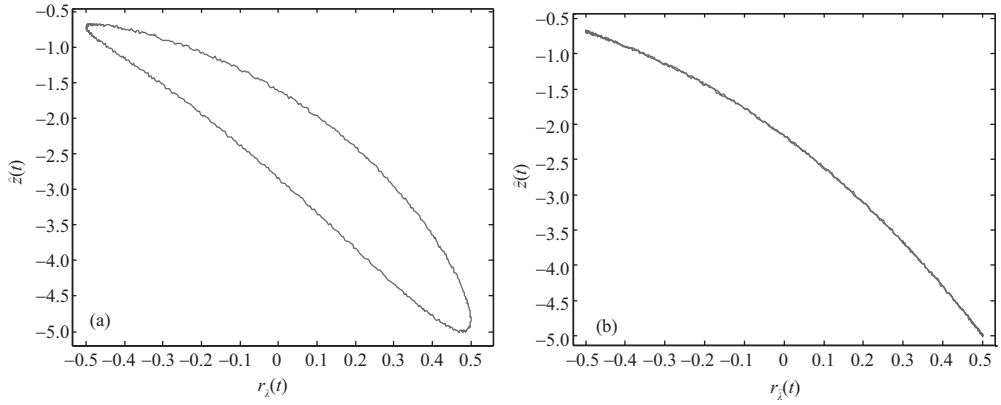

Figure 21 (a) Curve $\hat{C}_\lambda(\omega_2)$ for $\lambda = -0.04$ (rd) $\neq \varphi(\omega_2) \pm k\pi$; (b) curve $\hat{C}_{\bar{\lambda}_2}(\omega_2)$ for $\bar{\lambda} = -0.34$ (rd) $\approx \varphi(\omega_2)$ (modulo π).

Table 1 Results of linear bloc identification

Parameter	Value		
ω (rd/s)	0.05	0.1	0.5
$\varphi(\omega)$	-0.171	-0.3	-1.40
$\hat{\varphi}(\omega)$	-0.175	-0.346	-1.33
$\lvert G(j\omega)\rvert$	1	0.98	0.58
$\lvert \hat{G}(j\omega)\rvert$	1	0.96	0.62

static curve $\hat{C}_{\bar{\lambda}}(\omega)$, the parameter estimates $\hat{a}_k(\omega)$, for $k = 1\hat{a}n$, can be easily obtained. Finally, utilizing the estimator (23) the gain $|G(j\omega)|$, for any ω, can be determined. The gain $|\hat{G}(j\omega)|$ for $\omega = \omega_2$ and $\omega = \omega_3 = 0.5$ rd/s is provided by Table 1. The input nonlinearity identification is executed by following the steps outlined in Algorithm 3. Then, let us consider the reference signal $r_\lambda(t)$ in (13), where $\omega = \omega_1$, $U = 0.5$, and $\lambda = \bar{\lambda} = \hat{\varphi}(\omega_1)$. The system is excited by (12), where the offset u_o is initialized by $u_o = u_{\min} + U = -1.5$. Therefore, the obtained curve $\hat{C}_{\bar{\lambda}}(\omega_1) = \hat{f}(\hat{X}_1 + \hat{S}_1 r_{\bar{\lambda}}(t))$ is demonstrated by Figure 22. Then, $\hat{D}_1$ and $\hat{S}_1$ can be determined using (26a) and (26b). Subsequently, let us increase u_o until $\hat{C}_{\bar{\lambda}}(\omega_1)$ becomes nonstatic. This value of u_o is noted u_0^*, which is equal to -1.499. Figures 23 and 24 indicate the curve $(r_{\bar{\lambda}}(t), y(t))$ and its filtered version $\hat{C}_{\bar{\lambda}}(\omega_1)$, respectively. The same experiment is repeated for the other segments. For convenience, Figure 25 indicates a comparison between the true nonlinearity $h(\cdot)$ and its estimate $\hat{h}(\cdot)$.

These findings indicate that the estimated values are close to their true values. The obtained results indicate a good level of accuracy between the true nonlinear system and the estimated model, which verifies the performance of the proposed algorithm.

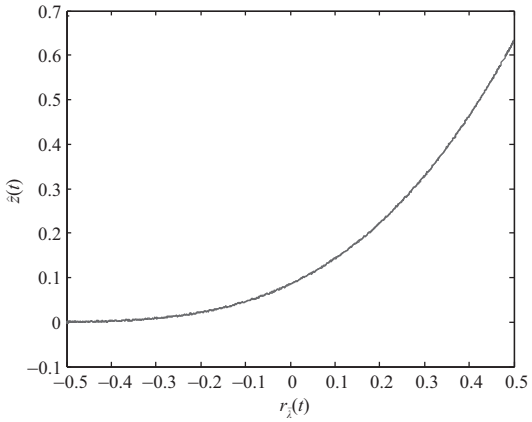

Figure 22 The curve $\hat{C}_{\bar{\lambda}}(\omega_1)$ for $u_o = -1.5$.

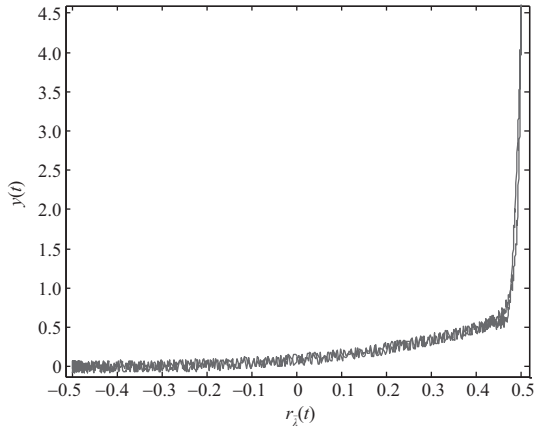

Figure 23 The curve $(r_{\bar{\lambda}}(t), y(t))$ over one period for $u_o = u_0^*$.

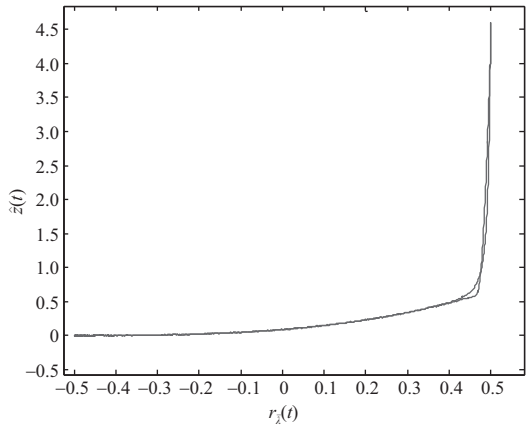

Figure 24 The curve $\hat{C}_{\bar{\lambda}}(\omega_1)$ for $u_o = u_0^*$.

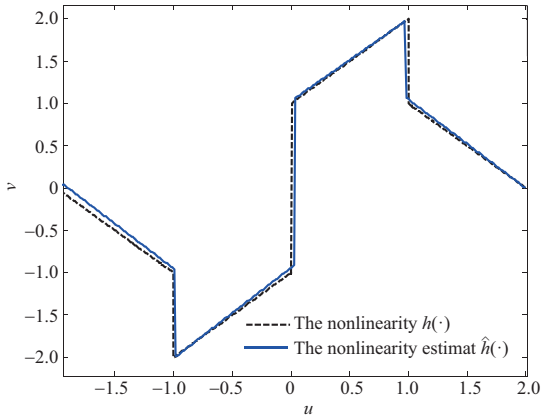

Figure 25 (Color online) Comparison between $h(\cdot)$ and $\hat{h}(\cdot)$ nonlinearities.

5 Conclusion

This paper addresses the identification challenge of Hammerstein-Wiener nonlinear systems. The originality of the present study lies in the fact that the input block is allowed to be discontinuous in addition to featuring a set of discontinuous linear segments. The output nonlinear block is described by a polynomial function that is not necessarily invertible. The problem of discontinuous nonlinearity has not been widely studied within the context of Hammerstein-Wiener systems. Additionally, the input nonlinearity exhibits several interesting and complex effects, for instance, dead zone, saturation, preload, and other effects. Note that the linear element can be parametric or nonparametric.

The obtained simulations revealed a good level of accuracy, which validated the performance of the established approach. To avoid multi-experiments, an identification solution using a multi-sine signal could be used.

References

1 Brouri A. Wiener-Hammerstein nonlinear system identification using spectral analysis. Int J Robust Nonlinear Control, 2022, 32: 6184–6204
2 Castro-Garcia R, Agudelo O M, Suykens J A K. Impulse response constrained LS-SVM modelling for MIMO Hammerstein system identification. Int J Control, 2019, 92: 908–925
3 Schoukens M, Tiels K. Identification of block-oriented nonlinear systems starting from linear approximations: a survey. Automatica, 2017, 85: 272–292
4 Brouri A, Kadi L. Identification of nonlinear systems. In: Proceedings of Conference SIAM CT'19, Chengdu, 2019. 22–24
5 Brouri A, Kadi L, Slassi S. Frequency identification of Hammerstein-Wiener systems with backlash input nonlinearity. Int J Control Autom Syst, 2017, 15: 2222–2232
6 Hsu K, Poolla K, Vincent T L. Identification of structured nonlinear systems. IEEE Trans Automat Contr, 2008, 53: 2497–2513

7 Novara C, Vincent T, Hsu K, et al. Parametric identification of structured nonlinear systems. Automatica, 2011, 47: 711–721
8 Chen H F. Recursive identification for Wiener model with discontinuous piece-wise linear function. IEEE Trans Automat Contr, 2006, 51: 390–400
9 Brouri A, Kadi L, Benyassi M. Identification of nonlinear systems having discontinuous nonlinearity. Int J Modelling Identif Control, 2019, 33: 130–137
10 Giri F, Rochdi Y, Brouri A, et al. Parameter identification of Hammerstein systems containing backlash operators with arbitrary-shape parametric borders. Automatica, 2011, 47: 1827–1833
11 Giri F, Rochdi Y, Radouane A, et al. Frequency identification of nonparametric Wiener systems containing backlash nonlinearities. Automatica, 2013, 49: 124–137
12 Giri F, Radouane A, Brouri A, et al. Combined frequency-prediction error identification approach for Wiener systems with backlash and backlash-inverse operators. Automatica, 2014, 50: 768–783
13 Palanthandalam-Madapusi H J, Ridley A J, Bernstein D S. Identification and prediction of ionospheric dynamics using a Hammerstein-Wiener model with radial basis functions. In: Proceedings of the American Control Conference, Portland, 2005. 5052–5057
14 Taringou F, Hammi O, Srinivasan B, et al. Behaviour modelling of wideband RF transmitters using Hammerstein-Wiener models. IET Circuits Devices Syst, 2010, 4: 282–290
15 Ouannou A, Giri F, Brouri A, et al. Parameter identification of switched reluctance motor using exponential swept-sine signal. IFAC-PapersOnLine, 2022, 55: 132–137
16 Śliwiński P. Nonlinear System Identification by Haar Wavelets. Berlin: Springer-Verlag, 2013. 210
17 Bai E W. Identification of linear systems with hard input nonlinearities of known structure. Automatica, 2002, 38: 853–860
18 Brouri A, Ouannou A, Giri F, et al. Identification of parallel Wiener-Hammerstein systems. IFAC-PapersOnLine, 2022, 55: 25–30
19 Brouri A, Kadi L, Lahdachi K. Identification of nonlinear system composed of parallel coupling of Wiener and Hammerstein models. Asian J Control, 2022, 24: 1152–1164
20 Wills A, Schön T B, Ljung L, et al. Identification of Hammerstein-Wiener models. Automatica, 2013, 49: 70–81
21 Brouri A, Chaoui F Z, Giri F. Identification of Hammerstein-Wiener models with hysteresis front nonlinearities. Int J Control, 2022, 95: 3353–3367
22 Brouri A, Giri F, Ikhouane F, et al. Identification of Hammerstein-Wiener systems with backlash input nonlinearity bordered by straight lines. IFAC Proc Volumes, 2014, 47: 475–480
23 Giri F, Brouri A, Amdouri O, et al. Frequency identification of Hammerstein-Wiener systems with piecewise affine input nonlinearity. IFAC Proc Volumes, 2014, 47: 10030–10035
24 Ni B, Gilson M, Garnier H. Refined instrumental variable method for Hammerstein-Wiener continuous-time model identification. IET Control Theor Appl, 2013, 7: 1276–1286
25 Schoukens M, Bai E, Rolain Y. Identification of Hammerstein-Wiener systems. In: Proceedings of the 16th IFAC Symposium on System Identification, 2012. 274–279
26 Wang D, Ding F. Extended stochastic gradient identification algorithms for Hammerstein-Wiener ARMAX systems. Comput Math Appl, 2008, 56: 3157–3164
27 V́oŕos J. An iterative method for Hammerstein-Wiener systems parameter identification. Int J Control, 2010, 83: 1117–1124
28 Cerone V, Razza V, Regruto D. One-shot set-membership identification of generalized Hammerstein-Wiener systems. Automatica, 2020, 118: 109028
29 Vincent T L, Novara C. Mixed parametric/non-parametric identification of systems with discontinuous nonlinearities. Automatica, 2013, 49: 3661–3669
30 Li F, Jia L. Parameter estimation of Hammerstein-Wiener nonlinear system with noise using special test signals. Neurocomputing, 2019, 344: 37–48
31 Mzyk G, Biegański M, Mielcarek P. Multi-level identification of Hammerstein-Wiener systems. IFAC-PapersOnLine, 2019, 52: 174–179